HIPPOCAMPUS 26:816–831 (2016)

Nogo-A Controls Structural Plasticity at Dendritic Spines by Rapidly Modulating Actin Dynamics

Yves Kellner,[1] Steffen Fricke,[1] Stella Kramer,[2,3] Cristina Iobbi,[1] Corette J. Wierenga,[4] Martin E. Schwab,[2,3] Martin Korte,[1,5] and Marta Zagrebelsky[1]*

ABSTRACT: Nogo-A and its receptors have been shown to control synaptic plasticity, including negatively regulating long-term potentiation (LTP) in the cortex and hippocampus at a fast time scale and restraining experience-dependent turnover of dendritic spines over days. However, the molecular mechanisms and the precise time course mediating these actions of Nogo-A are largely unexplored. Here we show that Nogo-A signaling in the adult nervous system rapidly modulates the spine actin cytoskeleton within minutes to control structural plasticity at dendritic spines of CA3 pyramidal neurons. Indeed, acute Nogo-A loss-of-function transiently increases F-actin stability and results in an increase in dendritic spine density and length. In addition, Nogo-A acutely restricts AMPAR insertion and mEPSC amplitude at hippocampal synaptic sites. These data indicate a crucial function of Nogo-A in modulating the very tight balance between plasticity and stability of the neuronal circuitry underlying learning processes and the ability to store long-term information in the mature CNS. © 2016 Wiley Periodicals, Inc.

KEY WORDS: actin cytoskeleton; AMPA receptor insertion; FRAP; neurite-growth inhibitors; structural plasticity

INTRODUCTION

Changes in synaptic connectivity involving growth and retraction of dendritic spines and axonal boutons—structural plasticity—have been correlated to functional changes at synapses (Yuste and Bonhoeffer, 2001) and are thought to underlie learning and memory processes (Caroni et al., 2012). Yet, long-term in vivo imaging performed after the end of the critical period in several sensory systems reveals that the overall morphology of axons and dendrites, including subpopulations of synaptic structures is remarkably stable (Holtmaat and Svoboda, 2009). These observations suggest the need for a set of molecules regulating the balance between stability and plasticity of mature neuronal networks, ensuring the spatial and temporal specificity of plastic changes and preventing interference between different memory events (Bavelier et al., 2010).

The membrane protein Nogo-A, originally identified as a myelin-associated neurite growth inhibitor is known for its role in limiting axonal regeneration and compensatory fiber growth and in preventing functional recovery after injury in the adult central nervous system (CNS) (for a review see Schwab, 2010). More recently, Nogo-A and its receptors, the Nogo-66 receptor 1 (NgR1) (Fournier et al., 2001), the sphingosine 1-phosphate receptor 2 (S1PR2) (Kempf et al., 2014) and the Paired-immunoglobulin-like receptor B (PirB) (Atwal et al., 2008) have been shown to be expressed pre- and post-synaptically in brain areas typically characterized by high plasticity levels, e.g. cerebral cortex and hippocampus (Liu et al., 2003; Lee et al., 2008; Kempf et al., 2014). Important physiological functions of Nogo-A signaling have been identified in restricting the dendritic and axonal architecture of mature hippocampal pyramidal neurons (Zagrebelsky et al., 2010; Petrinovic et al., 2013) and in negatively regulating activity-dependent synaptic plasticity by specifically limiting the height of LTP in the adult intact hippocampus and motor cortex (Lee et al., 2008; Delekate et al., 2011; Mironova and Giger, 2013; Kempf et al., 2014; Zemmar et al., 2014). Moreover, mutations of Nogo-A, NgR1, and PirB has been shown to limit experience-driven plasticity at the end of the critical period in the visual cortex (McGee et al., 2005; Syken et al., 2006). While recent work indicates that NgR1 limits ocular dominance and tactile task performance independent of basal anatomical plasticity (Park et al., 2014; Frantz et al., 2015) in some studies, NgR1 and PirB have been shown to modulate experience-dependent turnover of dendritic spines and axonal varicosities in the somatosensory and visual cortex (Akbik et al., 2013; Djurisic et al., 2013) over days or weeks leaving this question still open. Whether Nogo-A acutely regulates structural plasticity in the hippocampus, at a time scale comparable to its effects on activity-dependent functional synaptic plasticity remains so far

[1] **Division of Cellular Neurobiology, Zoological Institute, Braunschweig, Germany;** [2] **Brain Research Institute, University of Zurich, Zurich, Switzerland;** [3] **Department of Health Sciences and Technology, ETH Zurich, Zurich, Switzerland;** [4] **Division of Cell Biology, Faculty of Science, Utrecht University Utrecht, Netherlands;** [5] **Helmholtz Centre for Infection Research, AG NIND, Braunschweig, Germany**

Additional Supporting Information may be found in the online version of this article.

Grant sponsor: Deutsche Forschungsgemeinschaft; Grant number: ZA 554/3-1 (to M.Z. and M.K.); Grant sponsor: Advanced ERC Grant ("NOGORISE"); Grant number: 294115; Grant sponsor: Swiss National Science Foundation; Grant number: 31-138676 and 3100A0_12252711 (to M.E.S.).

*Correspondence to: Marta Zagrebelsky, Division of Cellular Neurobiology Zoological Institute, TU Braunschweig Spielmannstrasse. 7 D-38106 Braunschweig, Germany. E-mail: m.zagrebelsky@tu-bs.de

Accepted for publication 28 December 2015.
DOI 10.1002/hipo.22565
Published online 7 January 2016 in Wiley Online Library (wileyonlinelibrary.com).

unknown. We show here that Nogo-A signaling acutely controls actin cytoskeleton dynamics to restrict structural plasticity at individual dendritic spines of CA3 hippocampal pyramidal neurons on a fast time scale (minutes). In parallel, we observe that Nogo-A acutely restricts AMPAR insertion both under basal conditions and upon LTP induction providing a possible mechanism for its ability to negatively regulate excitatory synaptic transmission in CA3 pyramidal neurons. These results identify Nogo-A as an important molecular modulator of activity-dependent functional and structural plasticity at hippocampal synapses in the mature intact CNS.

MATERIAL AND METHODS

Neuronal Cultures

Preparation of hippocampal organotypic slice cultures

Hippocampal organotypic cultures were prepared from postnatal day 5 (P5) C57Bl/6 mice of either sex as previously described (Stoppini et al., 1991; Michaelsen-Preusse et al., 2014). All procedures concerning animals were approved by the animal welfare representative of the TU Braunschweig and the LAVES (Oldenburg, Germany, Az. §4 (02.05) TSchB TU BS). After decapitation the hippocampi were dissected in ice-cold sterile Gey's balanced salt solution (GBSS) and sliced transversally at a thickness of 400 μm. The slices were placed on Millicells CM membrane inserts (Millipore) and cultivated in a 37°C, 5% CO_2, 99% humidity environment in a medium containing 50% BME (Eagle, with Hanks salts without glutamine), 25% Hank's Buffered Salt Solution (HBSS), 1% glucose, 25% donor equine serum (HyClone), and 0.5% L-glutamine. A mixture of antimitotic drugs (cytosine arabinoside, uridine, and fluorodeoxyuridine; 10^{-6} to 10^{-7} M each) was applied for 24 h 3 days after preparation.

Preparation of primary hippocampal cultures

Primary hippocampal cultures were prepared from Wistar rats or C57Bl/6 mice at embryonic day 18. Embryos were decapitated and the brains were kept in ice-cold phosphate buffer saline (PBS) containing 14 mM glucose and adjusted to pH 7.2. The dissected hippocampi were incubated for 10 min in trypsin/EDTA at 37°C and then mechanically dissociated. Cells were plated at a density of 10^5/well on poly-L-lysine-coated coverslips (12 mm) and kept in Neurobasal medium (Invitrogen) supplemented with 2% B27 (Invitrogen), 1% Gentamycin (Gibco), and 1% Glutamax at 37°C, 5% CO_2, and 99% humidity.

Acute Hippocampal Slices

Acute hippocampal slices were prepared from 8 weeks old C57BL/6 mice. The mice were euthanized with CO_2, decapitated and the brain was dissected and incubated for 3 min into 4°C carbogenated (95% O_2, 5% CO_2) high magnesium (Mg^{2+}) artificial cerebrospinal fluid (ACSF) containing 125 mM NaCl, 2.5 mM KCl, 1.25 mM NaH_2PO_4, 2 mM $MgCl_2$, 26 mM $NaHCO_3$, 2 mM $CaCl_2$, and 25 mM glucose. Both hippocampi were dissected and 400 μm thick transversal slices were cut with a vibratome (VT 1000S, Leica, Nussloch, Germany). The slices were maintained at room temperature for at least 90 min in a submerged storage chamber with carbogenated high Mg^{2+} ACSF before being used.

Transfection

Particle-mediated gene transfer

Individual neurons were biolistically transfected with an expression plasmid for a farnesylated form of eGFP, specifically targeted to the membrane, driven by the cytomegalovirus (CMV) promoter (eGFP-F; Clontech). Purified plasmids were precipitated onto 0.6 μm gold microcarrier particles according to the Helios Gene Gun (Bio-Rad) instruction manual. Hippocampal slice cultures were transfected after 14 to 16 days in vitro (DIV) using the Helios Gene Gun System (Bio-Rad). The gold beads coated with expression plasmids were shot with a pressure of 80 to 100 psi and a filter, with a pore size of 3 μm was used to prevent clusters from reaching the slices. The organotypic cultures were used for time-lapse imaging 5 to 7 days after transfection.

Single cell electroporation

CA3 pyramidal cells in 20 to 22 DIV hippocampal slice cultures were electroporated using the Axoporator 800A (Axon Instruments/Molecular Devices Corp.) under an upright fluorescence microscope (Zeiss examiner) equipped with a differential interference contrast (DIC) video camera as previously described (Michaelsen-Preusse et al., 2014). A total DNA concentration of 150 ng/μL was used for eGFP-ß-actin (eGFP-actin) and for the co-electroporation equal amounts of eGFP-actin and mCherry-F (Clontech). The slices were kept in sterile HBSS and electroporated with one train of 5 V, 200 Hz, 100 ms, square pulses of 1 ms. The tip resistance of the electrode (GC150F-10, O.D. 1.5 mm × I.D. 0.86 mm, Harvard Apparatus (Kent): tip diameter 1–2 μm) was 5 to 10 MΩ at a pressure of 10 to 20 mbar controlled by a pressure gauge (GDH200, Greisinger). The slices were used for Fluorescence recovery after photobleaching (FRAP) measurements 24 to 48 h later. Completely labeled, non-overlapping CA3 pyramidal neurons without any sign of degeneration were selected for imaging.

Transfection of primary hippocampal neurons

Rat primary hippocampal neurons were transfected at 10 DIV with Lipofectamine 2000 with a construct expressing superecliptic pHluorin tagged AMPA-receptor subunit GluR1 (Addgene, plasmid #24000; Kopec et al., 2006) according to manufacturer's protocol. Mouse primary hippocampal neurons were co-transfected with a plasmid driving the expression of mApple to label the neurons and with a plasmid driving the expression of eGFP tagged Nogo-A by a truncated CMV

promoter. After 50 min incubation the transfection medium was exchanged for the original Neurobasal medium. The cells were used 24 to 48 h after transfection.

Antibody and Chemical Blocker Treatment

The loss-of-function for the Nogo-A signaling was obtained using: (1) a monoclonal Nogo-A specific, function blocking antibody, against an 18-aa peptide in the most active region of Nogo-A (mouse IgG1, 11C7; Oertle et al., 2003; Liebscher et al., 2005; Maier et al., 2009; gift from Novartis Pharma AG, Basel, Switzerland to Martin Schwab); (2) a function-blocking antibody against the Nogo receptor NgR (goat anti-Nogo receptor affinity-purified goat IgG; R&D Systems); (3) a specific blocker for the sphingosine-1-phosphate receptor 2 (S1PR2; JTE-013; Tocris, 5 μM in DMSO); (4) a selective inhibitor of the Rho-associated protein kinase p160ROCK (Y27632 dihydrochloride, Tocris, 100 μM in H_2O); (5) the specific actin stabilizing agent Jasplakinolide (Tocris, 0.2 μM in DMSO). A mouse IgG1 antibody against Bromodeoxyuridine (anti-BrdU) was used as control for the Nogo-A and NgR blocking antibodies. All antibody solutions were freshly diluted to a final concentration of 5 μg/mL in imaging ACSF containing BSA (0.01%). For inhibitors solved in DMSO or H_2O, an equal amount of solvent was used as control. The gain-of-function for Nogo-A was obtained via the application of the Nogo-A active peptide NiG-Δ20 (300 nM; Oertle et al., 2003). Siliconized tubing were used and prewashed with ACSF containing BSA (0.01%) to prevent sticking of the antibodies (Chen et al., 1999). The perfusion rate in the imaging chamber was kept constant at 1 ml/min. The different control conditions (BSA, mouse IgG1 anti-BrdU antibody, DMSO, and H_2O) did not show any significant differences, for spine density and morphology, as well as in the FRAP experiments. Thus, cells treated with BSA and mouse IgG1 anti-BrdU antibody were pooled for the analysis of dendritic spine turnover and size (Figs. 1 and 2).

Penetration of Monoclonal Anti-Nogo-A Abs Into Organotypic Slice Cultures

DIV 21 organotypic hippocampal cultures were incubated in mouse anti-Nogo-A Ab 11C7 or a mouse IgG1 control antibody against Bromodeoxyuridine (anti-BrdU) diluted at 5 μg/mL for either 20 min or 3 h and then fixed in phosphate-buffered 4% Paraformaldehyde. After washing, the slices were incubated overnight at 4°C with a Cy3-conjugated goat anti-mouse IgG Fcγ subclass 1-specific Ab (1:200; Jackson ImmunoResearch). After washing, the slices were incubated in DAPI solution to counterstain the nuclei. The distribution of the anti-Nogo-A mouse IgGs within the tissue was imaged with an Olympus, BX61WI FluoView 1000 laser scanning confocal microscope (Supporting Information Fig. S1).

Imaging

Time-lapse imaging

The organotypic slice cultures were transferred to an open imaging chamber at 32°C and continuously perfused (1 mL/min) with ACSF (in mM: 124 NaCl, 4.9 KCl, 25.6 $NaHCO_3$, 2 $MgCl_2$*$6H_2O$, 2 $CaCl_2$*$2H_2O$, 1.2 KH_2PO_4, 10 D-glucose; pH 7.4; saturated with carbogen) and let adapt for 30 min before imaging. Confocal image stacks of second-order mid-apical dendritic branches of eGFP-F expressing CA3 cells were acquired before and after treatment at intervals of 20 or 60 min up to 3 h using laser scanning confocal microscope (Olympus, BX61WI FluoView 1000). A 60× water objective (NA1.0) and a z-step size of 0.35 μm were used. The image size was 1,024 × 256 pixels for a final pixel size of 47 nm. To capture rapid dynamic events upon Nogo-A-Δ20 peptide application, stacks of 20 to 25 optical sections (512 × 128 pixel, final pixel size 71 nm) were collected every minute for 20 min. Two images were taken before application of the peptide for baseline measurement.

Fluorescence Recovery After Photobleaching (FRAP)

Only spines with an obvious head clearly separated from the dendrite and of equal size were used. The slices were kept at 32°C in an open imaging chamber with a continuous perfusion of ACSF (as above) for 30 min before starting the experiment. A confocal laser scanning microscope (Olympus, BX61WI FluoView 1000, FV1000) was used to excite eGFP-ß-actin with a laser power adjusted to 1 to 2%; 5 to 8 μW. A 60× water immersion objective (NA 1.0) was used with a scan speed set to 8 μs per pixel and a line averaging of two for a final pixel size of 76 nm. The photobleaching of a single spine was performed using the SIM scanner unit Olympus FV5-LDPSU at an excitation wavelength of 405 nm and a power of 28 to 32% (2.3 to 3 mW) for 28 to 30 ms. The pinhole was set to 400 μm. Five images were taken at 2 s intervals before and for 55 s after bleaching. Neighboring spines were monitored to ensure that only the spine of interest was bleached and to evaluate the stability of fluorescence. Imaging of the spine morphology was done with mCherry-F with a scanning speed of 12.5 μs, a line averaging of 2 and a final pixel size of 60 nm. Steps of 0.35 μm in *z* were used (maximum 15 to 20 *z*-planes). When combining FRAP and imaging of the morphology, the FRAP was performed first and then the spine morphology imaging for the selected dendrite at 20 and 180 min after treatment.

AMPAR insertion during glycine-induced chemical LTP (cLTP)

Hippocampal primary cultures were treated with Nogo-A blocking or control antibody (anti-BrdU) either acutely added to the medium or for 30 min before cLTP induction. Cells were transferred to a Ludin chamber (Life Imaging Services), and perfused with HEPES-buffered ACSF containing the antibodies preheated to 37°C for 30 min before the experiment. Cells were imaged every 5 min using a Leica TCS SP5 confocal inverted microscope (Leica Microsystems). Surface expression was visualized using the 488 nm laser line, with a 63× objective (oil immersion, NA 1.4) to a final pixel size of 50 nm using an 8,000 Hz Resonant scanner and HyD detectors (Leica Hybrid detectors). The cells were perfused with 4-(2-hydroxyethyl)-1-

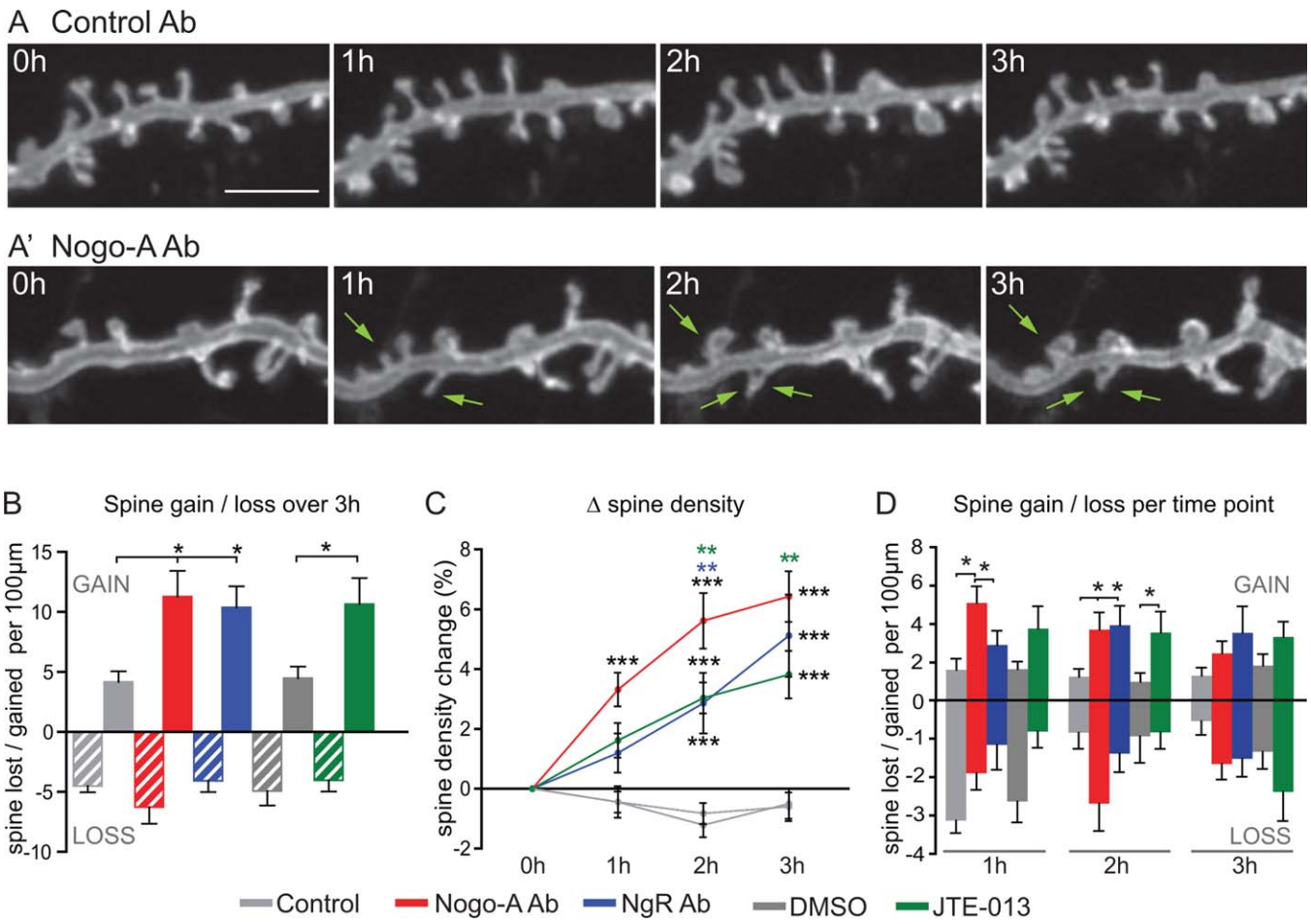

FIGURE 1. Nogo-A signaling acutely restricts dendritic spine turnover in CA3 pyramidal neurons. (A) Repeated confocal imaging of 3 weeks old eGFP-F expressing CA3 pyramidal neurons reveals a high degree of stability in dendritic spine number during control antibody treatment and an increase in the number of gained spines (green arrows) upon Nogo-A neutralization (A') over 3 h (3 h). Scale bar 5 µm. (B) Average number of spines lost or gained over 3 h imaging per 100 µm of dendritic length for controls (BSA-BrdU and DMSO), Nogo-A Ab, NgR Ab, and JTE-013 treatment. (C) Change (Δ) in dendritic spine density relative to the first time point (0 h) shown as percent of the 0 h value for controls (BSA-BrdU Ab and DMSO), Nogo-A Ab, NgR Ab, and JTE-013 treatment. The black asterisks indicate the significance between control and Nogo-A Ab, while the green and the blue asterisks indicate the significance between Nogo-A Ab and JTE-013 and NgR Ab respectively. (D) Time course of the average number of spines lost or gained over each hour of imaging per 100 µm of dendritic length for controls (BSA-BrdU Ab and DMSO), Nogo-A Ab, NgR Ab and JTE-013 treatment. Data are presented as mean ± SEM. *$P < 0.05$, **$P < 0.01$; ***$P < 0.001$. [Color figure can be viewed in the online issue, which is available at wileyonlinelibrary.com.]

piperazineethanesulfonic acid- (HEPES-) buffered ACSF (in mM: NaCl, 140; $CaCl_2$, 1.3; KCl, 5.0; HEPES, 25; glucose, 33; strychnine, 0.001; and bicuculline methiodide, 0.02, pH 7.4; Lu et al., 2001), and 0.01% BSA. For a pH 6.0—ACSF, HEPES was substituted with 25 mM 2-(N-morpholino)ethanesulfonic acid (MES) and buffered to pH 6.0. After 30 min adaptation three baseline images were taken at 5 min intervals followed by a 3 min wash in of a cLTP-inducting solution (HEPES-buffered ACSF with glycine; 200 µM).

Patch Clamp

Somatic whole-cell recording was performed on visually identified pyramidal neurons in the CA3 area in 16 to 21 DIV organotypic hippocampal cultures. The slices were transferred to an open imaging chamber at 35°C and were continuously perfused (1 ml/min) with ACSF (containing in mM 126 NaCl, 3 KCl, 26 $NaHCO_3$, 1.25 NaH_2PO_4, 1.3 $MgCl_2$*$6H_2O$, 2.5 $CaCl_2$*$2H_2O$, 20 D-glucose*H_2O; pH 7.4) saturated with carbogen and supplemented with 1 µM tetrodotoxin, 10 µM bicuculline, 50 µM AP5 and in control experiments also with 20 µM CNQX. The control antibody (anti-BrdU) or the Nogo-A function blocking antibody (11C7) were diluted in ACSF containing 0.01% BSA at a concentration of 5 µg/mL. The slices were let adapt for 30 min before starting recording. Glass pipette electrodes (resistance: 4.5–5.0 MΩ) were pulled with a PC-10 vertical micropipette puller (Narishige) from borosilicate capillaries. The pipette internal solution contained (in mM) 140 K-gluconate, 1 KCl, 10 HEPES, 0.5

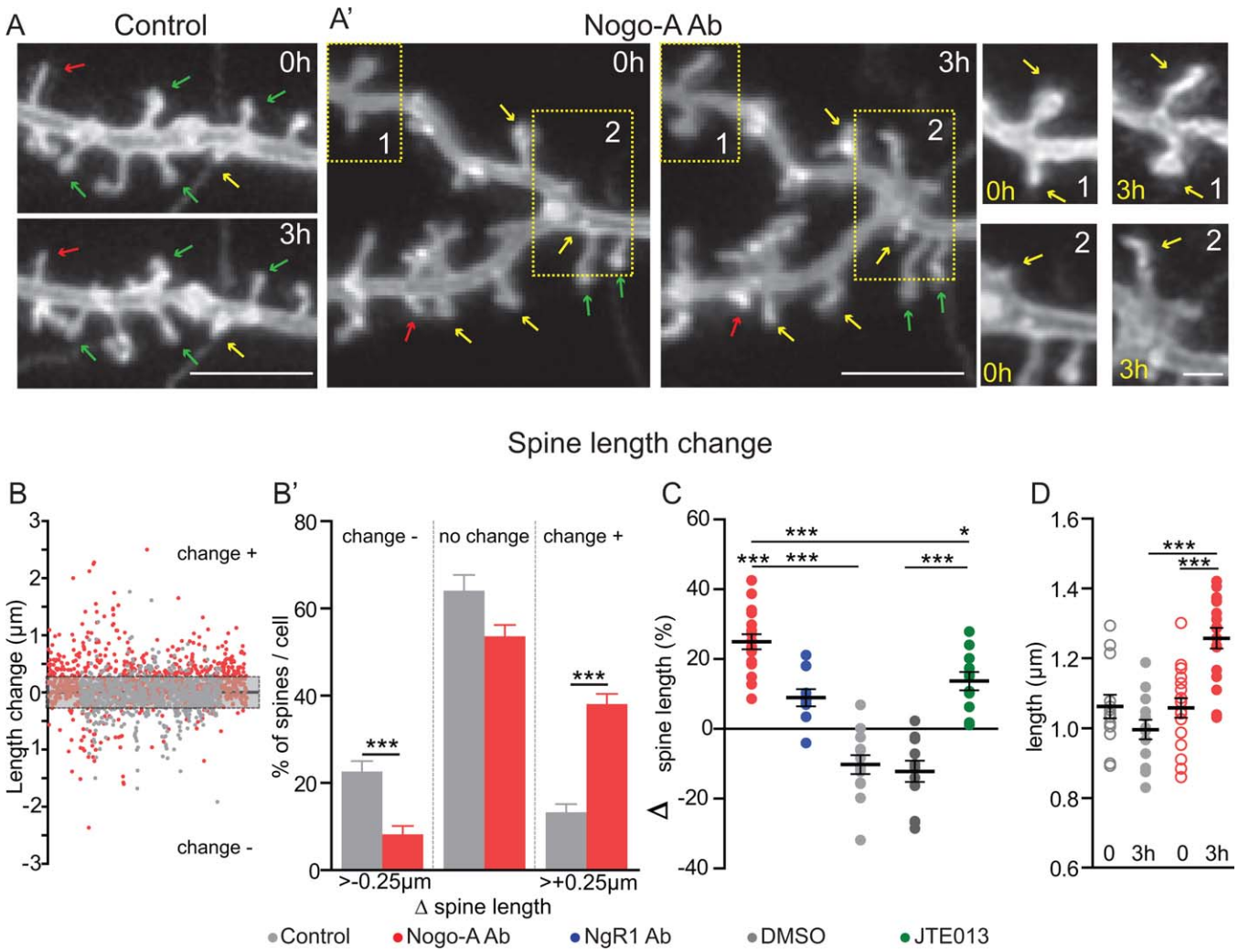

FIGURE 2. Nogo-A signaling acutely regulates dendritic spine architecture in CA3 pyramidal neurons. (A) Repeated confocal imaging of eGFP-F expressing CA3 pyramidal neurons reveals a high degree of stability of dendritic spine architecture upon control antibody treatment and a net elongation of dendritic spines (yellow arrows) upon 3 h Nogo-A neutralization (A'). Scale bars 5 µm. Green arrows indicate stable spines, red arrows indicate spines becoming shorter and yellow arrows indicate spines becoming longer. The inserts show two examples of elongating spines upon a 3 h Nogo-A Ab treatment. Scale bar 1 µm. (B) Scatter plot showing the change in length of single spines upon a 3 h control (gray) or Nogo-A blocking antibody (red) treatment. The gray shaded area shows the spines changing less than 250 nm in positive and negative. These are defined as not changing spines. (B') Graph showing the binning of dendritic spines according to their absolute length change (in µm) for control (BSA-BrdU Ab) and Nogo-A Ab treatments. Spines changing less than 250 nm in positive and negative are defined as not changing spines. Shortening (change −) and elongating (change +) spines are defined as the decrease or increase of more than 250 nm respectively. (C) Average spine length change (Δ) shown as percent of the initial value (0 h) for controls (BSA-BrdU Ab and DMSO), Nogo-A Ab, NgR Ab, and JTE-013 treatment. (D) Absolute dendritic spine length before and 3 h after treatment application for control (BSA-BrdU Ab) and Nogo-A Ab. Data are presented as mean ± SEM. *$P < 0.05$; ***$P < 0.001$. [Color figure can be viewed in the online issue, which is available at wileyonlinelibrary.com.]

EGTA, 4 MgATP, 0.4 Na_2GTP, 4 phosphocreatine (pH 7.3). Targeted patching was performed under an Olympus BX61W1 microscope using a 60× water-immersion objective (LUMPlanFL NA 1.00). To record miniature excitatory postsynaptic currents cells were voltage-clamped at −60 mV and mEPSCs recorded every 5 min for 3 min intervals up to 30 min after antibody application. Baseline mEPSC amplitude and frequency were 23.5 ± 1.34 pA and 0.46 ± 0.06 Hz for control conditions and 21.69 ± 1.11 pA and 0.37 ± 0.08 Hz for Nogo-A neutralization. Input resistance (R_{in}) and series resistance (R_s) were monitored over the recordings and only stable cells (<20% change in R_{in} and R_s) with $R_{in} > 100$ MΩ and $R_s < 30$ MΩ were included in the analysis. Signals were amplified using a Multiclamp 700B amplifier (Molecular Devices) and digitized with a Digidata 1440A digitizer (Molecular Devices). Data analysis was performed with the pClamp 10 software (Molecular Devices). The data are presented

as mean ± standard error of the mean (SEM). Statistical analysis was performed with Graph Pad Prism 5 using an ANOVA with Bonferroni post hoc test for multiple comparisons. Number of analyzed cells and frequency and amplitude values are reported in Supporting Information Table S4. Values of $P < 0.05$ were considered significant and plotted as follows $^*P < 0.05$.

Western Blot Analysis and Quantification of Cofilin Phosphorylation

Six to eight acute hippocampal slices were pooled in different groups and treated by bath application for 1 h with the following antibodies: a mouse polyclonal Nogo Receptor, NgR antibody, Cat. # AF1440, R&D Systems; a Nogo-A specific blocking antibody, antibody 11C7 mIgG1; a control antibody, anti BrdU mIgG1. The treated slices were homogenized in 1% Chaps based lysis buffer (30 mM Tris-Cl at pH 7.5, 150 mM NaCl, 1% Chaps) containing Protease Inhibitor (Complete protease inhibitor cocktail tablets, Roche) and Phosphatase Inhibitor (PhosSTOP phosphatase inhibitor cocktail tablets, Roche), and the debris were pelleted by centrifugation (15,000×g for 15 min at 4°C). Protein concentration was measured via Bradford assay and 100 μg of proteins per lane were loaded, separated onto 4 to 12% NuPAGE Bis-Tris Mini Gels (Invitrogen), and transferred onto a PVDF membrane by using a semi-dry blot. The membrane was blocked with 5% BSA in TBS-Tween for 1 h at RT and incubated at 4°C ON with the following primary antibodies diluted in 3% BSA in TBS-Tween: anti-Cofilin (1:10,000, ab11062, Abcam), anti-phospho-Cofilin (1:500, ab12866, Abcam), and anti-α-Tubulin, (1:10.000, #9026, Sigma-Aldrich). The membrane was washed in tris-buffered saline/Tween and incubated for 1 h at RT with the respective HRP conjugated secondary antibodies (Sigma-Aldrich). Immunoreactivity was detected by chemoluminescence (Luminata Crescendo Western HRP substrate, Millipore). After detection of p-Cofilin the blot was stripped and reprobed for total Cofilin. For quantification each sample was run independently at least two times. The relative optical density of the immunoreactive bands was analyzed with ImageJ software and α-Tubulin was used as loading control. The control treatment was set to 1, and the ratio phospho-protein to total protein was normalized to the control. The statistical analysis was performed by using GraphPad Prism with a one-way Anova and Bonferroni's post hoc test for multiple comparisons. All data are shown as mean ± SEM. Values of $P < 0.05$ were considered significant and plotted as follows $^*P < 0.05$.

Data Analysis

Analysis of dendritic spine density and morphology

Images were deconvolved using AutoQuantX2 (Media cybernetics, Inc.) and analyzed with ImageJ (US National Institutes of Health). The analysis was done blind to the treatment. Dendritic spines were classified as dendrite protrusions of at least 0.5 μm and no longer than 3 μm. Spine density over consecutive time points was measured in three dimensions by determining the number of spines per unit of length (μm) using the segmented line and the multipoint selection tools to measure dendritic length and count spine number, respectively. Spine density change between time points is shown as change in % relative to the spine density at the first time point. Gained and lost spines are shown in percent and are defined as the number of gained or lost spines per 100 μm of dendrite either per time point or as a total over the 3 h imaging. Morphometric analysis of dendritic spines was done in three dimensions using the segmented line tool of ImageJ to measure spine length (from the base at the dendrite to its tip) and head width (measured at its maximum). Positive and negative spine length changes are shown as % indexed to the respective initial values. Taking into account the resolution limit of 234 nm of the used imaging system, the analysis of dendritic spine morphology was performed on spines whose length and head width changed more than 250 nm during the 3 h of imaging. For the analysis of the role of the NiG-Δ20 peptide on dendritic spine length and head width the data at the different time points are shown as average values normalized to the time point before peptide application.

Statistical analysis of changes in spine density, spine length, and head width was performed per cell using a repeated measures analysis of variance (ANOVA) followed by a Bonferroni post hoc test for multiple comparisons. Number of analyzed spines, cells and slice cultures are reported in Supporting Information Tables S1 and S2. Two-way comparisons were made by two-tailed paired Student's *t*-test. All data are shown as mean ± standard error of the mean (SEM).

Analysis of the FRAP experiments

Images were analyzed using the Olympus software FV1000, by drawing regions of interest (ROI) around the bleached spine as previously described (Star et al., 2002; Michaelsen-Preusse et al., 2014). For the background and bleaching correction four ROIs were placed next to the bleached spine and on the underlying dendrite, respectively. The average relative intensity of the ROIs was calculated, the mean background fluorescence was subtracted and a double normalization was performed (Phair et al., 2004). The background corrected mean intensity values for each time were plotted against time. The fluorescent intensity of each time point was normalized to the average value derived from five pre-bleaching images (relative fluorescence). Nonlinear curve fitting was performed in GraphPad Prism where the net recovery after photobleaching is provided by the following equation: $Y = Y_0 + (\text{Plateau} - Y_0) \times (1 - \exp(-K \times x))$ where Y_0 is the Y value directly after the bleaching impulse. The Plateau is the Y value at infinite times, expressed as a fraction of the fluorescence before bleaching and was used to determine the dynamic actin pool. The stable actin pool is the fraction of fluorescence which does not recover within the imaging period and is calculated as 1-(F-actin dynamic), K is the rate constant, Tau is the time constant, expressed in seconds, computed as the reciprocal of K. From this equation, the actin turn-over time was calculated as the time at which 50% recovery of pre-bleaching fluorescence levels was reached. No significant differences could be seen in the mean spine head width of spines selected for the FRAP upon the different treatments. The statistical analysis and nonlinear

curve fitting of the fluorescence intensity were done per spine using GraphPad Prism 5 by a two-way repeated analysis of variance (ANOVA) inter-subject test followed by a two-tailed Student's *t*-test. Number of spines, cells, and slice cultures used are reported in Supporting Information Table S3. For the actin fractions and the turnover time an unpaired two-tailed Student's *t*-test was used. Values of $P < 0.05$ were considered significant and plotted as follows $^{*}P < 0.05$; $^{**}P < 0.01$; $^{***}P < 0.001$. All data are indicated as mean ± standard error of the mean (SEM).

Analysis of AMPAR insertion during glycine-induced cLTP

Three-dimensional image stacks were projected to two-dimensional images using maximal intensity and the resulting time-lapse stacks were aligned with the Stackreg tool of ImageJ, projected over time and duplicated. One copy was blurred (Gaussian blur 20) and subtracted from the other, smoothed image. After application of a fix threshold to all time points, ROIs were defined for synapses in the resulting image. The integrated intensity of the SEP-GluR1 signal on every spine was measured over time to calculate spine $\Delta F/F_0 T_o$. The fraction of synapses at which the fluorescence intensity increased by at least 100% 30 min after Nogo-A Ab application with or without cLTP was counted using ImageJ. Statistical significance was tested using repeated measures ANOVA. *P* values below 0.05 were considered significant. Number of analyzed cells and $\Delta F/F_0 T_o$ values are reported in Supporting Information Table S4.

RESULTS

Blocking Nogo-A Signaling Acutely Affects Dendritic Spine Turnover

To assess the contribution of Nogo-A signaling in regulating dendritic spine turnover confocal laser scanning microscopy was combined with a series of specific loss-of-function approaches in three-week-old organotypic hippocampal slice cultures. Repeated imaging of eGFP-F expressing mid-apical CA3 dendrites over 3 h under control conditions revealed a stable dendritic spine number (Fig. 1A). While both spine losses and gains were observed (Fig. 1B) no obvious changes in dendritic spine density over time could be detected (Fig. 1C, Supporting Information Table S1). Application of Nogo-A function blocking antibodies (Nogo-A Ab) resulted in an increase in the formation of new spines already apparent 1 h after treatment (Fig. 1A', green arrows) without increasing spine loss. Indeed, while the number of gained dendritic spines per 100 μm of dendrite was significantly increased ($P < 0.05$) when compared with the control, the number of lost spines was only slightly higher (Fig. 1B) resulting in a gradual, significant increase in dendritic spine density relative to the time point before treatment (1–3 h $p < 0.001$; Fig. 1C). The increase in gained spines was significant 1 and 2 h ($P < 0.05$) but not at 3 h after Nogo-A Ab treatment (Fig. 1D, Supporting Information Table S1) suggesting a fast and transitory effect of the Nogo-A loss-of-function.

The actions of Nogo-A are due to the signaling of two inhibitory extracellular domains: Nogo-66 signaling via the Nogo-66 receptor 1 (NgR1) (Fournier et al., 2001) and Nogo-A-Δ20 signaling via the Sphingosine 1-phosphate receptor 2 (S1PR2) (Kempf et al., 2014). Blocking the function of either Nogo-A receptor alone resulted in a progressive increase in dendritic spine density which became significantly higher than the controls after 2 h (2 h and 3 h $p < 0.001$; Fig. 1C, Supporting Information Table S1). The increase in spine density was due to a significant increase in new spine formation ($P < 0.05$) without significant changes in dendritic spine loss (Figs. 1B, D; Supporting Information Table S1). However, this increase remained significantly lower than upon Nogo-A Ab treatment (2 h $P < 0.01$ NgR Ab, JTE-013; 3 h $P < 0.01$ JTE-013; Fig. 1C). These observations point to the combined action of the two Nogo-A receptors, NgR1 and S1PR2 in regulating spine turnover on a fast time scale in mature hippocampal neurons.

Nogo-A Blocking Antibody Penetration

Nogo-A Ab penetration to a depth of 60 to 100 μm into acute hippocampal slices was previously confirmed immunohistochemically (Zemmar et al., 2014). However, to show that during the application time the Nogo-A Ab indeed penetrated the organotypic slice cultures to a depth at which the eGFP-F positive cells were located (around 30 μm), at the end of the incubation time treated slice cultures were immunohistochemically processed to stain mouse IgG1s. Already 20 min after Nogo-A Ab application a signal was detected in several somas (Supporting Information Figs. S1A, A', A"; arrows) and along the main apical and basal dendrites (Supporting Information Figs. S1A, A" arrowheads) of CA3 pyramidal neurons at a depth at which some eGFP-F expressing cells are located (Supporting Information Figs. S1A–A", yellow arrow). After 3 h of treatment many labeled neurons were observed within the *stratum pyramidale* (Supporting Information Figs. S1B, B', sp) with many labeled dendrites within the *stratum radiatum* (Supporting Information Figs. S1B, B", sr) of the CA3 region of slices treated with Nogo-A, but not with control antibodies (Supporting Information Fig. S1D). Indeed, labeled Nogo-A Ab could be detected both within the soma (Supporting Information Fig. S1C, red arrows) and along the main apical dendrites (Supporting Information Fig. S1C, red arrowheads) of CA3 pyramidal neurons. To further analyze the subcellular distribution of Nogo-A and confirm its localization within dendritic spines, primary hippocampal neurons were transfected to co-express mApple to visualize the neuronal architecture and low levels of eGFP tagged Nogo-A driven by a truncated CMV promoter. Nogo-A-eGFP was clearly localized within both the proximal and the distal dendrites (Supporting Information Fig. S2A, open arrowheads) as well as within the axon (Supporting Information Fig. S2A, filled arrowheads). Nogo-A and its

receptor, NgR1 were previously shown to be located both pre- and post-synaptically in the hippocampus (Lee et al., 2008). Indeed, we could observe Nogo-A-eGFP expression in most dendritic spines (Supporting Information Fig. S2A' insert, arrows) of mApple labeled hippocampal neurons.

Nogo-A Signaling Modulates Dendritic Spine Architecture at a Fast Time Scale

To assess whether Nogo-A signaling is involved in regulating structural plasticity at dendritic spines we first analyzed dendritic spine length. At a qualitative level under control conditions, while most dendritic spines were stable over time (Fig. 2A, green arrows) a few spines showed either a reduction (red arrows) or an increase in length (yellow arrows). In contrast, upon 3 h Nogo-A neutralization more spines changed over time. Of the changing spines, fewer became shorter (Fig. 2A' red arrows, 2B) and more became longer (Fig. 2A' and inserts yellow arrows, 2B). Next, the changes in length of individual spines along the dendrites were quantified both for control and Nogo-A-Ab treated slice cultures. Under both conditions the majority of spines underwent a change in length below 250 nm and was therefore classified as not changing (Figs. 2B, B'). However, while in control treated cells length changes greater than 250 nm could be observed in $36.46 \pm 3.78\%$ of spines, upon Nogo-A Ab treatment the percentage of changing spines was significantly higher ($47.34 \pm 2.74\%$; $p < 0.05$; Figs. 2B, B'). Moreover, in comparison with the control upon Nogo-A Ab application significantly more of the changing dendritic spines elongated (Fig. 2B'; $P < 0.001$) while significantly less shortened relative to their initial length (Fig. 2B'; $P < 0.001$). While spines of control treated cells showed on average a decrease in length of about 10% over the 3 h of imaging, in Nogo-A Ab treated cells spine length significantly increased on average of about 25% of the initial value (Fig. 2C; $P < 0.001$) resulting in a net increase in absolute dendritic spine length upon 3 h Nogo-A neutralization (Fig. 2D; $P < 0.001$) but not under control conditions. Dendritic spine elongation was already significantly higher than in controls after 100 min of treatment with Nogo-A Ab (Supporting Information Fig. S3A; $P < 0.01$). In control cells longer spines (>1 μm initial length) were usually shortening and shorter spines (≤1 μm initial length) showed only slight elongation over time (Supporting Information Fig. S3B and Supporting Information Table S2). Upon Nogo-A neutralization when compared with controls, longer spines became significantly shorter and a significantly higher increase in length was observed for initially shorter spines (Supporting Information Fig. S3B; $P < 0.001$ and 0.01) indicating that Nogo-A neutralization equally affects both longer and shorter spines.

To address the role of the NgR1 and S1PR2 receptors in mediating this effect of Nogo-A, dendritic spine length changes were assessed in CA3 pyramidal neurons treated with a loss-of-function approach for either one of the two receptors. Blocking the function of either NgR1 or S1PR2 resulted in a significant dendritic spine elongation relative to the respective controls (Fig. 2C; $P < 0.001$; Supporting Information Table S2), although the increase was for both significantly lower than the one observed upon Nogo-A Ab treatment (Fig. 2C; $P < 0.001$ for NgR Ab and $P < 0.05$ for JTE013; Supporting Information Table S2). This suggests that Nogo-A controls dendritic spine length signaling through both receptors, with the largest contribution of S1PR2.

Next we addressed a possible role of Nogo-A signaling in regulating dendritic spine head width. Blocking Nogo-A function resulted in only a slightly higher proportion of spines whose head was enlarging above the 250 nm threshold (Supporting Information Fig. S3C, C' and Supporting Information Table S2). Moreover, average spine head width slightly, but not significantly increased after 3 h treatment when compared with the control treated cells (Supporting Information Fig. S3D). Together these data implicate fast Nogo-A signaling in modulating dendritic spine morphology, with a specific effect on spine length.

Nogo-A Controls Actin Dynamics Within Single Dendritic Spines

Filamentous actin is highly concentrated in dendritic spines and plays an important role in regulating spine morphology, size, and number (Matus, 2000; Okamoto et al., 2009). To test whether Nogo-A signaling is involved in regulating actin dynamics, we performed fluorescence recovery after photobleaching (FRAP) at individual spines of eGFP-actin expressing CA3 pyramidal neurons (Fig. 3A) 20 min and 3 h after applying different loss- or gain-of-function treatments. Fluorescence was stable throughout the experiment in neighboring spines and before bleaching (Figs. 3B, C). Upon bleaching, fluorescence specifically and completely disappeared in single spines (Fig. 3A), followed by gradual recovery to about 85% of the prebleaching fluorescence level (Fig. 3B), which is consistent with previous reports (Star et al., 2002) and indicates that under control conditions, most of the actin within spines exists in a dynamic state. FRAP measurements performed 20 min after Nogo-A Ab application resulted in significantly lower intensity values during the entire fluorescence recovery curve (Fig. 3B; $P < 0.01$). Accordingly, under Nogo-A neutralization both the stable actin fraction and the turnover time were significantly increased (Figs. 3B', B"; Supporting Information Table S3; $P < 0.05$ and $P < 0.001$). At 3 h after Nogo-A neutralization, while the fluorescence recovery curve was significantly altered (Fig. 3C; $P < 0.05$) and the turnover time significantly higher (Fig. 3C"; $P < 0.05$), the stable actin fraction was comparable to control levels (Fig. 3C'; Supporting Information Table S3). Similar to blocking Nogo-A function, a 20 min application of NgR Ab shifted the fluorescence recovery curve to lower values (Fig. 3B; $P < 0.001$) with a significant increase in the actin stable fraction (Fig. 3B'; $P < 0.001$) and turnover time ($P < 0.01$; Fig. 3B'). After 3 h of NgR Ab the fluorescence recovery curve was significantly lower (Fig. 3C; $P < 0.05$) and the turnover time was significantly higher than in controls (Fig. 3C'; $P < 0.01$). Instead, the stable actin fraction was now comparable to the control values (Fig. 3C'). The effects of the S1PR2 receptor blocker JTE-013 seemed to last longer than blocking either Nogo-A or NgR1. When

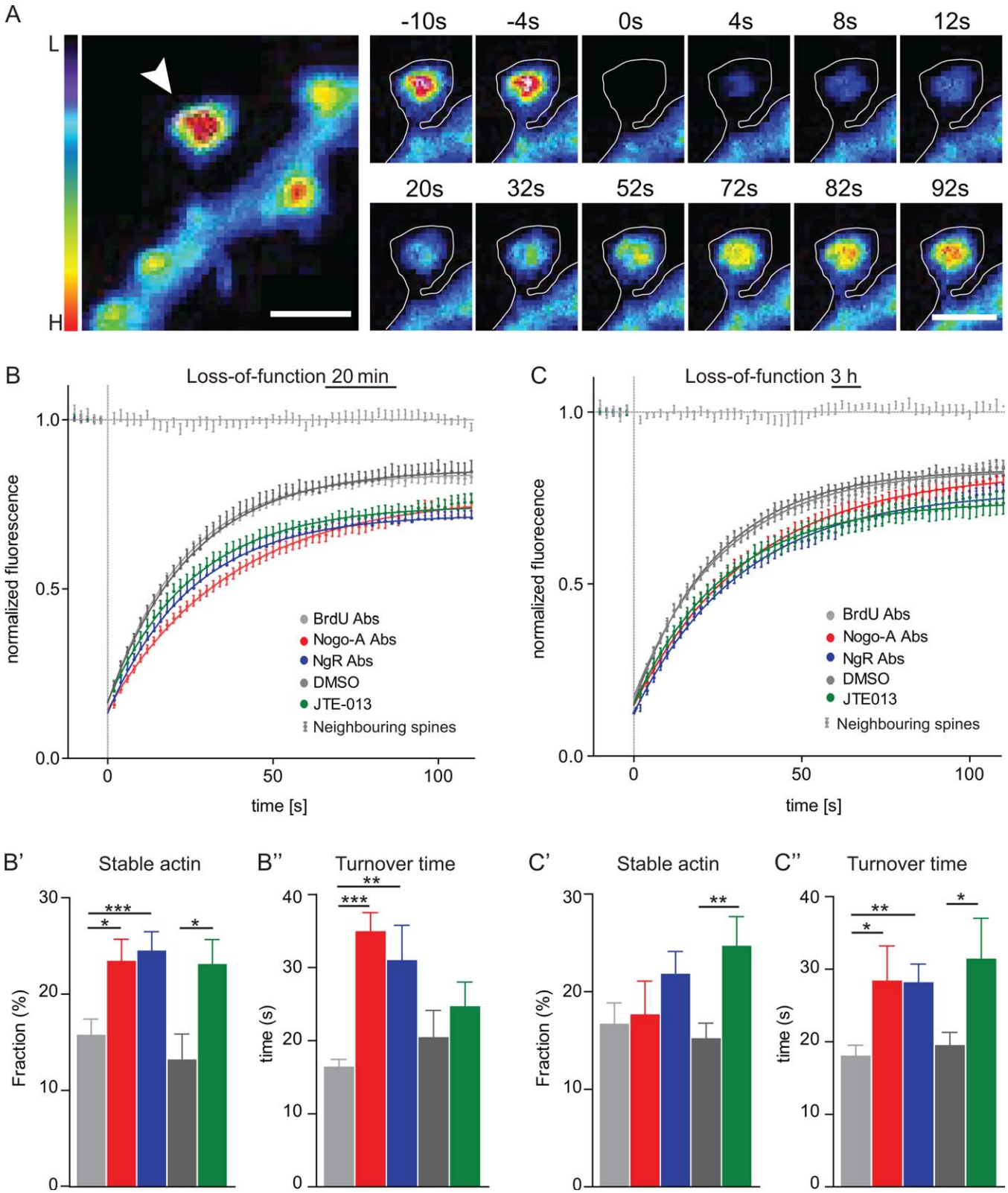

FIGURE 3. Nogo-A signaling acutely and transiently regulates actin dynamics within single dendritic spines. (A) Pseudocolored micrograph showing eGFP-actin accumulation at dendritic spines. Scale bar 2 μm. Repetitive imaging of one single dendritic spine (white arrowhead) before and after bleaching (0 s is the time point of bleaching). Scale bar 1 μm. The bar on the left shows the pseudocolor range (L low and H high). (B) Non-linear regression curve showing the average fluorescence recovery after photobleaching for eGFP-actin at single dendritic spines 20 min after application of different loss-of–function approaches: Nogo-A Ab, NgR Ab, and JTE-013 in comparison to the controls (BrdU Ab and DMSO) and (C) after 3 h. The light gray lines show the stability of fluorescence in spines neighboring the bleached ones at 20 min and 3 h. (B') Analysis of stable-actin fraction and turnover time (B") after 20 min of Nogo-A Ab, NgR Ab, and JTE-013 versus the controls (BrdU Ab and DMSO) or (C', C") after 180 min. Data are presented as mean ± SEM. *$P < 0.05$, **$P < 0.01$;*$P < 0.001$. [Color figure can be viewed in the online issue, which is available at wileyonlinelibrary.com.]**

the S1PR2 was blocked for 20 min, the fluorescence recovery curve was significantly lower (Fig. 3B, $P < 0.05$) and the stable actin fraction was significantly increased (Fig. 3B'; $P < 0.05$) compared with controls. These differences could still be observed after 3 h of JTE-013 application (Figs. 3C, C'; $P < 0.01$) when also the turnover time was significantly increased (Fig. 3C"; $P < 0.05$). Both NgR1 and S1PR2 have been shown to signal via the small GTPase RhoA and its effector the Rho-associated, coiled-coil-containing protein kinase (ROCK) (Niederost et al., 2002; Kempf et al., 2014). Interestingly, blocking the activity of ROCK by application of the specific inhibitor Y27632 results in a slight shift of the fluorescence recovery curve to lower values (Supporting Information Fig. S4A) with no changes in the turnover time (Supporting Information Fig. S4A') but in a significant increase in the stable actin fraction after 20 min of treatment (Supporting Information Fig. S4A"). Moreover, a 3-h application of Y27632 results in a significant increase in dendritic spine elongation (Supporting Information Fig. S4B) and in a slight increase in spine head width (Supporting Information Fig. S4B') similar to the one observed upon Nogo-A signaling neutralization.

We next tested whether the ability of Nogo-A to regulate actin dynamics is contributing to its modulation of dendritic spine structural plasticity. Changes in actin dynamics associated to alteration in the morphology of individual spines upon Nogo-A neutralization were simultaneously analyzed in CA3 pyramidal neurons expressing both eGFP-actin and mCherry-F (Supporting Information Fig. S5A). FRAP experiments were performed at the start of the experiment and repeated after 3 h of Nogo-A Ab treatment for the same spines. The spines were then separated in not changing (Supporting Information Fig. S5E, spine1) and elongating (Supporting Information Figs. S5A, B, E spine 2). Within the population of not changing spines there were no differences in the fluorescence recovery curves before and upon 3 h Nogo-A Ab treatment (Supporting Information Fig. S5E spine 1, S5F). We found that in the elongating spines (Supporting Information Fig. S5E, spine 2), the fluorescence recovery curve after 3 h of Nogo-A Ab treatment was shifted to lower intensity values (Supporting Information Fig. S5F') and that the stable actin fraction was significantly increased during treatment (Supporting Information Fig. S5C; $P < 0.05$). Moreover, for all elongating spines we observed a significant positive correlation between the amount of stable actin and their increase in length (Supporting Information Fig. S5D; $R^2 = 0.45$; $P < 0.05$). These data suggest that Nogo-A loss-of-function modulates dendritic spine size and shape by rapidly stabilizing the spine actin cytoskeleton. The actin binding protein Cofilin has been shown to depolymerize actin filaments resulting in the destabilization of the actin cytoskeleton. Thus, we next assessed whether Nogo-A signaling might regulate Cofilin activity by analyzing changes in Cofilin phosphorylation upon a loss-of-function approach. Both the neutralization of Nogo-A and of NgR1 by a 1 hour treatment with specific function blocking antibodies to acute hippocampal slices significantly increased the levels of inactive, phosphorylated Cofilin (Supporting Information Fig. S4C lower panel; Nogo-A Ab + 50.48 ± 17.5%; NgR Ab + 41.63 ± 10.4%; $P < 0.05$), without affecting total protein levels (Supporting Information Fig. S4C, upper panel) thereby possibly resulting in the observed stabilization of the actin spinoskeleton upon Nogo-A signaling loss-of-function.

Nogo-A Gain-of-Function Results in a Fast Shortening of Spines and a Transient Destabilization of the Actin Cytoskeleton

Next we set out to confirm the specific role of Nogo-A in regulating dendritic spine structural plasticity using a gain-of-function approach. We applied the active inhibitory Nogo-A peptide, NiG-Δ20 (Oertle et al., 2003) and analyzed changes in average dendritic spine length and head width over time. The soluble NiG-Δ20 peptide is known to be rapidly internalized into neurons upon binding the S1PR2 forming a receptor-containing signaling endosome which is then rapidly degraded (Joset et al., 2010; Kempf et al., 2014) resulting in an acute gain-of-function followed by a delayed loss-of-function for Nogo-A signaling (Delekate et al., 2011). A 20 min application of NiG-Δ20 resulted in a fast and transient decrease in the average dendritic spine length relative to the time points before peptide application (Fig. 4A; $F_{(2,17)} = 9.93$; $P < 0.05$). When compared with the control treatment (Fig. 4A) average spine length was significantly reduced within the first 10 min of NiG-Δ20 application and returned to pretreatment values in the subsequent 10 min. Similarly, average dendritic spine head width was temporarily reduced relative to the time points before peptide application (Fig. 4A'; $F_{(2,17)} = 9.61$; $P < 0.01$). The growth cone collapsing activity of Nogo-A depends on its ability to activate the small GTPase RhoA and the downstream ROCK (Joset et al., 2010). While one hour pre-treatment with the Rho-associated, coiled-coil-containing protein kinase (ROCK) inhibitor Y27632 resulted only in a slight, not significant increase in dendritic spine elongation with no change in spine head width (Supporting Information Figs. S4B, B'), it completely prevented both the NiG-Δ20-induced spine shortening ($F_{(2,17)} = 9.93$; $P < 0.01$ to NiG-Δ20; Fig. 4A) as well as the spine head shrinkage ($F_{(2,17)} = 9.61$; $P < 0.01$ to NiG-Δ20; Fig. 4A'). These results are consistent with Nogo-A rapidly regulating dendritic spine size by modulating the dynamics of the actin cytoskeleton. Indeed, when FRAP was performed at eGFP-actin expressing spines just 5 min after NiG-Δ20 application, the fluorescence recovery curve was significantly shifted to higher intensity values (Fig. 4B; $P < 0.05$ from 10 to 110 s; Supporting Information Table S3). The stable actin fraction and turnover time (Figs. 4B', B"; $P < 0.05$, Supporting Information Table S3) were lower than in controls pointing to a destabilization of the actin cytoskeleton. In contrast, after 20 min NiG-Δ20 treatment fluorescence recovery curve was significantly shifted to lower intensity values (Fig. 4B) and the stable actin was significantly higher than in controls (Fig. 4B'; $P < 0.05$) as observed upon Nogo-A neutralization. These observation indicate a specific role of Nogo-A in regulating both dendritic spine size and dynamics of the actin cytoskeleton within spine heads. Finally, to confirm the role of Nogo-A gain-of-function in destabilizing the actin cytoskeleton and thereby inducing a shortening of dendritic spines, the Nogo-A NiG-Δ20 was co-applied together with the actin stabilizing agent Jasplakinolide. A 20 min application of both Jasplakinolide alone and in combination with NiG-

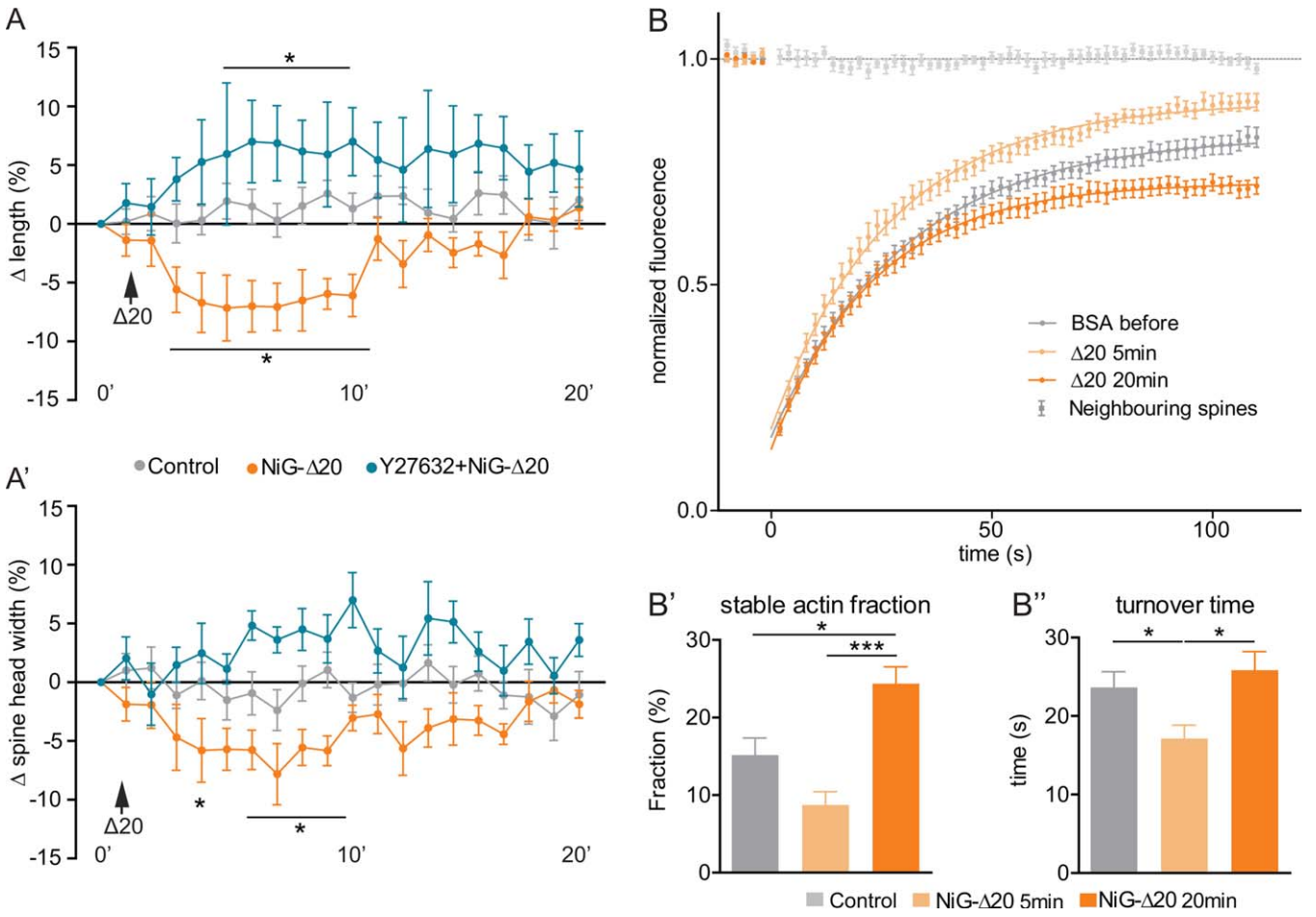

FIGURE 4. Nogo-A gain-of-function results in a transient spine shortening and actin destabilization (A). Average spine length and spine head width (A') normalized to the first time point (over 20 min) is shown for CA3 cells treated with control (gray), NiG-Δ20 (orange), or Y27632 and NiG-Δ20 (blue). (B) Nonlinear regression curves showing the fluorescence recovery after photobleaching for eGFP-actin at single spines 5 min (light orange) and 20 min (dark orange) after application of NiG- Δ20 versus control (BSA, gray). The light gray line shows the stability of fluorescence in spines neighboring the bleached ones. (B') Analysis of stable-actin fraction and turnover time (B") after 5 min (light orange) and 20 min (dark orange) NiG-Δ20 versus control (gray). Data are presented as mean ± SEM. *$P < 0.05$; ***$P < 0.001$. [Color figure can be viewed in the online issue, which is available at wileyonlinelibrary.com.]

Δ20 resulted in a slight, not significant increase in dendritic spine length without affecting dendritic spine width (Supporting Information Figs. S4D, D') thereby preventing the reduction observed in the length and head width observed for dendritic spines upon the application of NiG-Δ20 alone (Figs. 4A, A').

Taken together our data show that the fast signaling of Nogo-A leads to a transient destabilization of the actin cytoskeleton within spines and shortening of spines, while blocking Nogo-A signaling induces actin stabilization and spine elongation.

Nogo-A Limits AMPA Receptor Insertion

We next wanted to address if changes in spine morphology by fast Nogo-A signaling have functional consequences thereby influencing synaptic transmission at CA3 pyramidal neurons. Modulation of alpha-amino-3-hydroxy-5-methyl-4-isoxazolepropionic acid receptor (AMPAR) localization at the surface plays a crucial role in synaptic plasticity. Indeed, LTP is reflected by an actin-mediated increase in the number of postsynaptic AMPA receptors (O'Brien et al., 1998; Kim and Lisman, 1999). To investigate whether Nogo-A regulates AMPAR insertion at dendritic spines, we expressed super-ecliptic pHluorin fused to the N-terminus of the AMPAR subunit glutamate receptor 1 (SEP-GluR1, Miesenböck et al., 1998) in primary hippocampal neurons (Figs. 5A, A') and examined the dynamic changes in the density of surface SEP-GluR1. While 30 min exposure to control antibodies did not change SEP-GluR1 fluorescence, acute treatment with Nogo-A Ab resulted in a small, but progressive increase in SEP-GluR1 fluorescence within spines (Fig. 5B). Moreover, the number of SEP-GluR1 clusters whose fluorescence was augmented by 100% was significantly increased upon Nogo-A Ab when compared with the control conditions (Fig. 5B'; $P < 0.05$). To test whether Nogo-A regulates changes in surface AMPARs upon neuronal activity, we

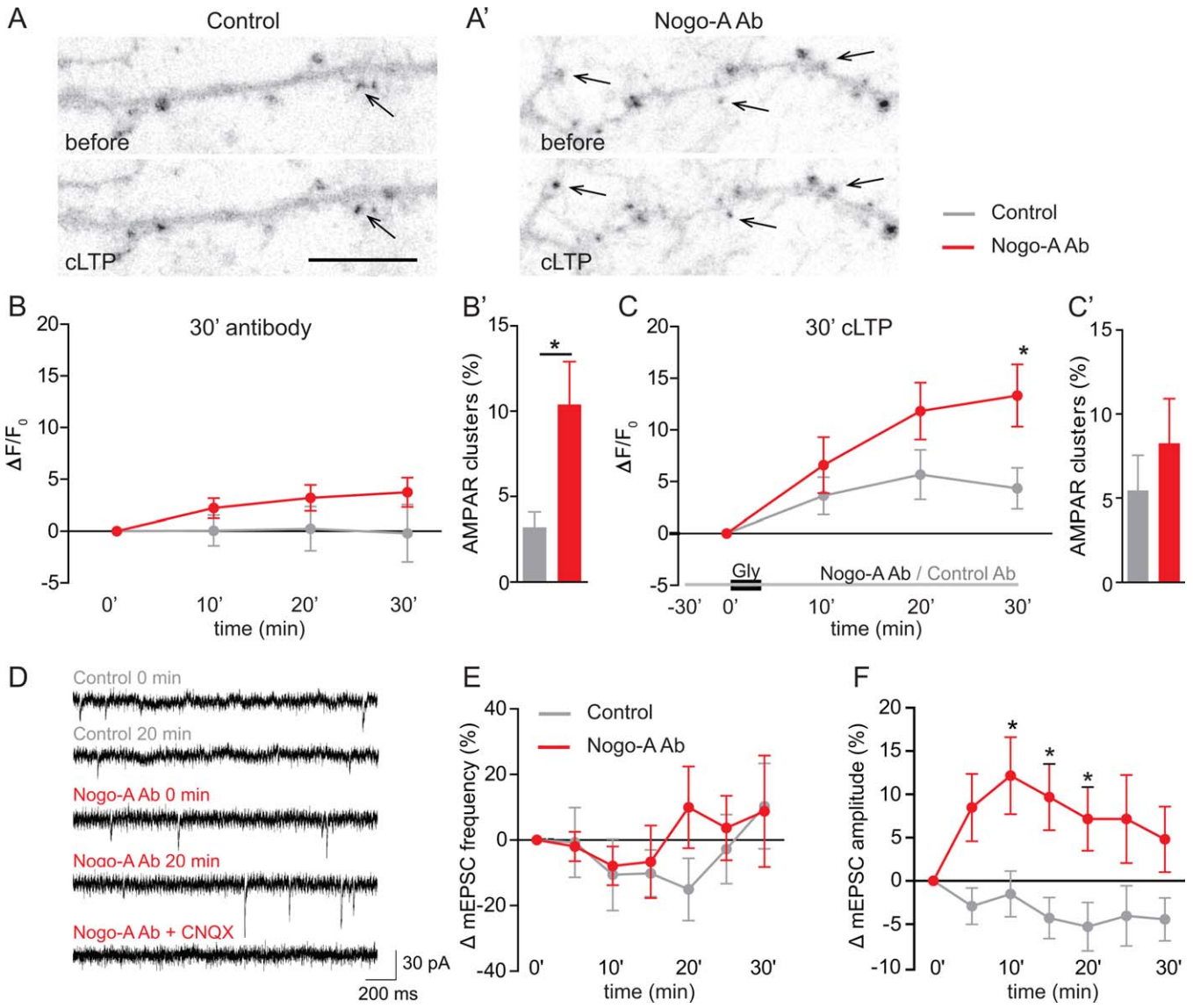

FIGURE 5. Nogo-A restricts AMPA receptor insertion and negatively modulates excitatory synaptic transmission. (A) Representative images showing SEP-GluR1 fluorescence on dendritic regions before (−10 min) and after (30 min) cLTP induction by a 3 min application of Glycine during control antibody treatment. (A') Representative images showing SEP-GluR1 fluorescence on dendritic regions before (−10 min) and after (30 min) cLTP induction during Nogo-A neutralization. Arrows indicate spines with marked SEP-GluR1 addition. Scale bar represents 5 μm. (B) Integrated intensity ($\Delta F/F_0$) of SEP-GluR1 fluorescence and number of AMPA receptor clusters whose fluorescence increased by 100% (B') over 30 min control (BrdU-Ab, gray) or Nogo-A Ab (red) treatment. (C) Integrated intensity ($\Delta F/F_0$) of SEP-GluR1 fluorescence and number of AMPA receptor clusters whose intensity increased by 100% (C') before and after cLTP induction in hippocampal primary neurons pretreated for 30 min with control (BrdU-Ab, gray) or Nogo-A Ab (black). (D) Depicted are representative traces of patch clamp recordings from CA3 pyramidal cells treated before and 20 min after the application of control or Nogo-A blocking antibody alone or with CNQX. (E) and (F) Show the change in percent of the frequency and amplitude of mEPSCs in control-Ab (gray) or Nogo-A Ab (red) treated CA3 pyramidal neurons relative to the time point before the antibodies were applied. Data are presented as mean ± SEM. *$P < 0.05$. [Color figure can be viewed in the online issue, which is available at wileyonlinelibrary.com.]

chemically induced LTP by a brief exposure of hippocampal neurons to Glycine. In neurons treated with control antibodies, cLTP induction resulted in a small increase in SEP-GluR1 fluorescence to a maximum of about 5% (Figs. 5A, C; $F_{(1,51)} = 6.19$; $P < 0.05$). Upon Nogo-A neutralization cLTP-induced fluorescence was increased to 15% (Figs. 5A', C; $F_{(17,51)} = 9.54$; $P < 0.01$) becoming significantly higher than in controls 30 min after cLTP induction ($P < 0.05$). The number of SEP-GluR1 clusters whose fluorescence was increased by 100% was slightly increased under both conditions (Fig. 5C').

Next, to corroborate the observed increase in density of AMPAR upon Nogo-A Ab treatment we tested whether this effect

is mirrored by an alteration in mEPSC amplitude or frequency at CA3 pyramidal neurons. Whole-cell patch-clamp recordings were performed to monitor mEPSCs in CA3 pyramidal neurons in organotypic hippocampal slice cultures. Nogo-A Ab treatment resulted in only a slight increase in the frequency of mEPSCs (Figs. 5D, E) 20 min after treatment when compared with the controls (Figs. 5D, E). On the contrary, mEPSC amplitude was significantly increased 10, 15, and 20 min after Nogo-A Ab application when compared with control conditions (Figs. 5D, F; $P < 0.05$). The mEPSCs measured upon Nogo-A loss-of-function were completely blocked by co-application of CNQX, confirming the role played by AMPARs in their generation (Fig. 5D).

These observations indicate that acutely blocking Nogo-A modulates synaptic AMPAR density and thereby the strength of excitatory synaptic transmission.

DISCUSSION

We show here that Nogo-A signaling can rapidly restrict spine actin dynamics and that this affects structural and functional plasticity at dendritic spines of CA3 pyramidal cells. Blocking Nogo-A signaling transiently increases F-actin stability within minutes and results in increased dendritic spine number and length, indicating that the actin spinoskeleton is under continuous control of Nogo-A signaling. Moreover, our data show that Nogo-A signaling regulates excitatory synaptic transmission possibly both directly by restricting AMPAR insertion and indirectly through changes in spine morphology.

Linking Structural and Functional Activity-Dependent Plasticity

Nogo-A and its receptors stabilize synaptic weight by negatively regulating activity-dependent synaptic plasticity (Lee et al., 2008; Delekate et al., 2011; Kempf et al., 2014; Zemmar et al., 2014). While the acute neutralization of Nogo-A or of its receptors NgR1 or S1PR2 results in higher LTP (Delekate et al., 2011; Kempf et al., 2014), a gain-of-function approach by the application of Nogo-A-Δ20 or Nogo-66 peptides reduces the amplitude of post-tetanic stimulation (Delekate et al., 2011) or LTP (Raiker et al., 2010). Induction of LTP is accompanied by a rapid insertion of AMPA receptors and by their increased clustering on the surface at synaptic sites (Lu et al., 2001; Huganir and Nicoll, 2013). SiRNA mediated down regulation of Nogo-A or NgR1 over three days has been shown to positively influence NMDAR and AMPAR levels through a rapamycin-sensitive mTOR-dependent translation mechanism (Peng et al., 2011). Moreover, experience-dependent delivery of AMPAR in the barrel cortex has been shown to persist in adult NgR1 knockout mice (Jitsuki et al., 2016). Here we show that acute neutralization of Nogo-A signaling induces a fast (within minutes) increase in the density of surface AMPA receptors in primary hippocampal neurons under basal activity as well as enhances AMPA receptor insertion at synapses upon chemical induction of LTP. These observations suggest that excitatory synaptic transmission in hippocampal neurons might be under constant control of Nogo-A. Indeed, the amplitude of mEPSCs recorded from CA3 pyramidal neurons increased rapidly upon acute treatment with Nogo-A neutralizing antibodies paralleling the observed increase in AMPAR density. While the observed increase in mEPSC amplitude with no change in mEPSC frequency suggests increased insertion of AMPARs at pre-existing sites, the formation of new AMPAR clusters cannot be excluded. Our observations provide evidence that Nogo-A signaling is involved in the fast regulation of excitatory synaptic transmission at hippocampal synapses. These results may appear to be in contradiction with previous reports showing no significant alteration in baseline synaptic transmission upon Nogo-A neutralization (Lee et al., 2008; Delekate et al., 2011; Zemmar et al., 2014). However, previous reports looked at a time scale of hours to days, while here we analyze the effects within min of a Nogo-A neutralization. Indeed, we found that the increase in mEPSC amplitude, spine turnover and the changes in actin dynamics within spines were transient, indicating that blocking Nogo-A signaling only transiently affects synaptic transmission. This suggests that additional control mechanisms exist for maintaining synaptic strength. While Nogo-A has been shown to be expressed both pre- and post-synaptically (Lee et al., 2008) in the hippocampus, our previous observations suggest that the Nogo-A restricts LTP through a purely postsynaptic mechanism (Delekate et al., 2011). Our current findings could indicate that the molecular composition of excitatory synapses may be different in the presence or absence of postsynaptic Nogo-A signaling. Interestingly, Nogo-A signaling has been shown to exert its action on the cytoskeleton *via* the regulation of cofilin activity (Hsieh et al., 2006; Montani et al., 2009). Moreover, temporally regulated ADF/cofilin activities are crucial for postsynaptic modifications of both AMPA receptor number and dendritic spine size during synaptic plasticity (Gu et al., 2010). We speculate that the ability of Nogo-A signaling to control excitatory transmission mediates its ability to restrict synaptic plasticity.

The collaborative interaction between functional and structural changes at synapses underlies long-lasting synaptic plasticity (Caroni et al., 2012). We show a role of Nogo-A signaling in modulating the number and architecture of post-synaptic structures at a time scale of minutes to hours matching its effect on excitatory synaptic transmission and the one reported on LTP (Delekate et al., 2011). An increase in the activity-dependent turnover of dendritic spines and axonal varicosities has been shown for the somatosensory cortex of NgR1 knockout mice (Akbik et al., 2013) and for the motor cortex of rats receiving Nogo-A neutralizing antibodies (Zemmar et al., 2014) suggesting that indeed Nogo-A and NgR1 signaling are involved in regulating anatomical plasticity upon learning. While previous reports relied on the analysis either of knockout mice or of rats chronically treated with function blocking antibodies over days, here we use an acute approach to neutralize Nogo-A signaling and show a surprisingly fast addition of new dendritic spines in mature CA3 hippocampal neurons. We currently don't know if accompanying changes at presynaptic structures occur (Akbik et al., 2013). The fast increase in spine

density associated with an increase in AMPA receptor clusters observed here suggests an increase in synapses upon Nogo-A neutralization. Furthermore, we observe a fast, significant increase in dendritic spine length and a slight increase in spine head width upon blocking Nogo-A signaling. On the contrary, upon Nogo-A gain-of-function both dendritic spine length and head width decrease. Spine head morphology has been shown to be dynamic and positively correlated to synaptic efficacy (Kasai, 2003). Moreover, their architecture has been shown to regulate the biochemical and electrical compartmentalization of dendritic spines (Tønnesen et al., 2014). An increase in spine neck length would increase electrical isolation of the spine heads from the dendrites (Yuste, 2013). In addition, an increase in dendritic spines length has been associated with increased spine motility (Zito et al., 2004). Together, this suggests that blocking Nogo-A signaling might reduce overall spine maturation. Indeed, Nogo-A signaling has been associated with the end of the critical period suppressing plasticity in the visual cortex at the end of its development (McGee et al., 2005). Furthermore, NgR1 (Josephson et al., 2003; Karlsson et al., 2013) as well as Nogo-A mRNA (Mingorance et al., 2004) have been shown to be transiently downregulated in the cortex and hippocampus of adult rodents under different situations associated with increased neuronal activity and plasticity, e.g. kainic acid administration, exposure to running wheels and sensory deprivation (Endo et al., 2007). In addition, an increase in neuronal activity within hippocampal primary neurons in vitro has been shown to reduce protein expression for members of the NgR family, known to restrict dendritic spine and synapse development (Wills et al., 2012). While the global regulation of Nogo-A and NgR1 by neuronal activity strongly indicates their role in regulating plastic processes, the important question of whether Nogo-A signaling might be regulated by neuronal activity at the level of single synapses remains to be addressed.

Actin Dynamics and Spine Architecture

Filamentous actin is the main constituent of the cytoskeleton in spines, and modulation of actin dynamics is the common denominator on which different signaling pathways converge to control spine morphology and synaptic strength (Cingolani and Goda, 2008). Both Nogo-A-Δ20 and Nogo-66 trigger the activation of the small GTPase RhoA and its effector ROCK resulting in growth cone collapse and axonal repulsion (Niederost et al., 2002; Kempf et al., 2014). Accordingly, inactivated RhoA is increased in *nogo-a* KO mice resulting in the deactivation of the actin severing protein cofilin and in increased actin polymerization supporting formation and extension of filopodia in growth cones (Montani et al., 2009). We show here that a regulation of actin dynamics similar to the one observed in growth cones also acts within mature dendritic spines to control their architecture and suppress structural plasticity at dendritic spines in the mature hippocampus. Neutralizing Nogo-A or its receptors NgR1 and S1PR2 in mature hippocampal neurons results in the fast stabilization of the actin cytoskeleton shown by an increase in turnover time and in the stable actin fraction already after 20 min. This stabilizing effect on the actin cytoskeleton is transient and is partially reversed after 3 h of treatment. The stabilization of the actin cytoskeleton is correlated to an increase in spine number and length. Interestingly, increased F-actin stabilization has been shown to be sufficient to promote spinogenesis and spine elongation (Zito et al., 2004). Furthermore, a gain-of-function approach for Nogo-A results in a fast destabilization of the actin cytoskeleton possibly associated by a ROCK activation-dependent shortening of dendritic pines. Similarly, in developing hippocampal neurons NgR1 restricts synaptic and dendritic growth through RhoA activation (Wills et al., 2012). Also, relevant to our results RhoA inactivation results in more and longer spines suggesting that it can repress the formation and elongation of spines (Tashiro et al., 2000). Down-regulation of the myosin light chain II, regulating the retrograde flow of G-actin has been observed in *nogo-a* KO mice (Montani et al., 2009) and its inhibition results in an increase both in spine number and length (Ryu et al., 2006). While we cannot exclude that inactivation of myosin light chain II might contribute to the effect of Nogo-A neutralization on dendritic spines, our data indicate that Nogo-A controls structural plasticity at spines by regulating actin dynamics most likely via the RhoA-ROCK pathway. One possible model explaining actin-powered growth and elongation for instance of filopodia is the "elastic Brownian ratchet model," in which the addition of new actin subunits at the barbed end of actin filaments pushes on the membrane (Mogilner and Oster, 1996; Pollard et al., 2000). Thus, a higher stabilization of actin filaments may result in larger protrusive forces and possibly in increased dendritic spine growth. This model is consistent with our observations of an increased formation (Fig. 1) and elongation of dendritic spines (Fig. 2) associated with the stabilization of the actin filaments (Fig. 3) upon Nogo-A neutralization, possibly via the inactivation of the actin depolymerizing protein Cofilin (Supporting Information Fig. S4C). Moreover, the model is supported by the observation that the shortening of spines observed upon a Nogo-A gain-of-function approach is associated with an increase in the actin dynamic pool within spines (Fig. 4) and prevented by the co-application of the actin stabilizing drug Jasplakinolide (Supporting Information Fig. S4D). Our results indicate that Nogo-A signaling controls dendritic spine number and structure on the same fast time scale as for its effect on functional synaptic plasticity via the regulation of the propensity of the actin cytoskeleton to change.

CONCLUSIONS

Our data designate a precise role of Nogo-A in controlling dendritic spine number and morphology, the dynamics of actin within dendritic spine heads as well as AMPAR density and mEPSC amplitude. These data provide a fundamental

mechanism for the action of Nogo-A in regulating both functional and structural aspects of synaptic plasticity and suggest an important role for it in modulating the tight balance between plasticity and stability critical to the proper function of the mature CNS in an ever changing environment. Overall, they suggest a physiological role for Nogo-A in restricting functional and structural synaptic plasticity, thereby participating in the fine-tuning of synapses which is a prerequisite for long-term memory storage.

Acknowledgments

The authors thank Diane Mundil for the outstanding technical assistance in preparing the organotypic hippocampal cultures and performing the biolistic transfection and single cell electroporation. The authors thank as well Hai Yin Hu and Gayane Grigoryan for their help in performing the patch clamp experiments.

REFERENCES

Akbik FV, Bhagat SM, Patel PR, Cafferty WBJ, Strittmatter SM. 2013. Anatomical plasticity of adult brain is titrated by Nogo Receptor 1. Neuron 77:859–866.

Atwal JK, Pinkston-Gosse J, Syken J, Stawicki S, Wu Y, Shatz C, Tessier-Lavigne M. 2008. PirB is a functional receptor for myelin inhibitors of axonal regeneration. Science 322:967–970.

Bavelier D, Levi DM, Li RW, Dan Y, Hensch T. 2010. Removing breaks on adult brain plasticity: From molecular to behavioural interventions. J Neurosci. 30:14964–14971.

Caroni P, Donato F, Muller D. 2012. Structural plasticity upon learning: Regulation and functions. Nat Rev Neurosci 13:478–490.

Chen G, Kolbeck R, Barde YA, Bonhoeffer T, Kossel A. 1999. Relative contribution of endogenous neurotrophins in hippocampal long-term potentiation. J Neurosci 19:7983–7990.

Cingolani La, Goda Y. 2008. Actin in action: the interplay between the actin cytoskeleton and synaptic efficacy. Nat Rev Neurosci. 9:344–356.

Delekate A, Zagrebelsky M, Kramer S, Schwab ME, Korte M. 2011. NogoA restricts synaptic plasticity in the adult hippocampus on a fast time scale. Proc Natl Acad Sci USA 108:2569–2574.

Djurisic M, Vidal GS, Mann M, Aharon A, Kim T, Ferrao Santos A, Zuo Y, Hübener M, Shatz CJ. 2013. PirB regulates a structural substrate for cortical plasticity. Proc Natl Acad Sci USA 110: 20771–20776.

Endo T, Spenger C, Tominaga T, Brené S, Olson L. 2007. Cortical sensory map rearrangement after spinal cord injury: fMRI responses linked to Nogo signalling. Brain 130:2951–2961.

Frantz MG, Kast RJ, Dorton HM, Chapman KS, McGee AW. 2015. Nogo receptor 1 limits ocular dominance plasticity but not turnover of axonal boutons in a model of amblyopia. Cereb Cortex, doi: 10.1093/cercor/bhv014

Fournier AE, GrandPre T, Strittmatter SM. 2001. Identification of a receptor mediating Nogo-66 inhibition of axonal regeneration. Nature 409:341–346.

Gu J, Lee CW, Fan Y, Komlos D, Tang X, Sun C, Yu K, Hartzell HC, Chen G, Bamburg JR, Zheng JQ. 2010. DF/cofilin-mediated actin dynamics regulate AMPA receptor trafficking during synaptic plasticity. Nat Neurosci 13:1208–1215.

Hisieh SH, Ferraro GB, Fournier AE. 2006. Myelin-associated inhibitors regulate cofilin phosphorylation and neuronal inhibition through LIM kinase and Slingshot phosphatase. J Neurosci 26: 1006–1015.

Holtmaat A, Svoboda K. 2009. Experience-dependent structural synaptic plasticity in the mammalian brain. Neuroscience 10(9): 647–58.

Huganir RL, Nicoll RA. 2013. AMPARs and synaptic plasticity: the last 25 years. Neuron 80:704–717.

Jitsuki S, Nakajima W, Takemoto K, Sano A, Tada H. Takahashi-Jitsuki A, Takahashi T 2016. Nogo receptor signaling restricts adult neural plasticity by limiting AMPA receptor delivery. Cereb Cortex 26(1):427–39.

Josephson A, Trifunovski A, Schéele C, Widenfalk J, Wahlestedt C, Brené S, Olson L, Spenger C. 2003. Activity-induced and developmental downregulation of the Nogo receptor. Cell Tissue Res. 311: 333–342.

Joset A, Dodd Da, Halegoua S, Schwab ME. 2010. Pincher-generated Nogo-A endosomes mediate growth cone collapse and retrograde signaling. J Cell Biol 188:271–285.

Karlsson TE, Koczy J, Brené S, Olson L, Josephson A. 2013. Differential conserted activity induced regulation of Nogo receptors (1-3), LOTUS and Nogo mRNA in mouse brain. PLoS One 8: e60892–e60911. doi: 10.1371/journal.pone.0060892.

Kasai H. 2003. Structure–stability–function relationships of dendritic spines. Trends Neurosci 26:360–368.

Kempf A, Tews B, Arzt ME, Weinmann O, Obermair FJ, Pernet V, Zagrebelsky M, Delekate A, Iobbi C, Zemmar A, Ristic Z, Gullo M, Spies P, Dodd D, Gygax D, Korte M, Schwab ME. 2014. The sphingolipid receptor S1PR2 is a receptor for Nogo-A repressing synaptic plasticity. PLoS Biol 12:e1001763.

Kim CH, Lisman JE. 1999. A role of actin filament in synaptic transmission and long-term potentiation. J Neurosci 19:4314–4324.

Kopec CD, Li B, Wei W, Boehm J, Malinow R. 2006. Glutamate receptor exocytosis and spine enlargement during chemically induced long-term potentiation. J Neurosci 26:2000–2009.

Lee H, Raiker SJ, Venkatesh K, Geary R, Robak La, Zhang Y, Yeh HH, Shrager P, Giger RJ. 2008. Synaptic function for the Nogo-66 receptor NgR1: Regulation of dendritic spine morphology and activity-dependent synaptic strength. J Neurosci 28:2753–2765.

Liebscher T, Schnell L, Schnell D, Scholl J, Schneider R, Gullo M, Fouad K, Mir A, Rausch M, Kindler D, Hamers FPT, Schwab ME. 2005. Nogo-A antibody improves regeneration and locomotion of spinal cord-injured rats. Ann Neurol 58:706–719.

Liu YY, Jin WL, Liu HL, Ju G. 2003. Electron microscopic localization of Nogo-A at the postsynaptic active zone of the rat. Neurosci Lett 346:153–156.

Lu W, Man H, Ju W, Trimble WS, MacDonald JF, Wang YT. 2001. Activation of synaptic NMDA receptors induces membrane insertion of new AMPA receptors and LTP in cultured hippocampal neurons. Neuron 29:243–254.

Maier IC, Ichiyama RM, Courtine G, Schnell L, Lavrov I, Edgerton VR, Schwab ME. 2009. Differential effects of anti-Nogo-A antibody treatment and treadmill training in rats with incomplete spinal cord injury. Brain 132:1426–1440.

Matus A. 2000. Actin-based plasticity in dendritic spines. Science 290:754–758.

McGee AW, Yang Y, Fischer QS, Daw NW, Strittmatter SM. 2005. Experience-driven plasticity of visual cortex limited by myelin and Nogo receptor. Science 309:2222–2226.

Michaelsen-Preusse K, Kellner Y, Korte M, Zagrebelsky M. 2014. Analysis of actin turnover and spine dynamics in hippocampal slice cultures. In: Bakota L, Brandt R, editors. Laser Scanning Microscopy and Quantitative Image Analysis of Neuronal Tissue Neuromethods, Vol. 87. Neuromethods. New York, NY: Springer New York. pp 189–217.

Miesenböck G, De Angelis DA, Rothman JE. 1998. Visualizing secretion and synaptic transmission with pH-sensitive green fluorescent proteins. Nature 394:192–195.

Mingorance A, Fontana X, Solé M, Burgaya F, Ureña JM, Teng FY, Tang BL, Hunt D, Anderson PN, Bethea JR, Schwab ME, Soriano E, del Río JA. 2004. Regulation of Nogo and Nogo receptor during the development of the entorhino-hippocampal pathway and after adult hippocampal lesions. Mol Cell Neurosci 26:34–49.

Mironova YA, Giger RJ. 2013. Where no synapses go: Gatekeepers of circuit remodeling and synaptic strength. Trends Neurosci 66:1–11.

Mogilner A, Oster G. 1996. Cell motility driven by actin polymerization. Biophys J 71:3030–3045.

Montani L, Gerrits B, Gehrig P, Kempf A, Dimou L, Wollscheid B, Schwab ME. 2009. Neuronal Nogo-A modulates growth cone motility via Rho-GTP/LIMK1/cofilin in the unlesioned adult nervous system. J Biol Chem 284:10793–10807.

Niederost B, Oertle T, Fritsche J, McKinney RA, Bandtlow CE, Niederöst B. 2002. Nogo-A and myelin-associated glycoprotein mediate neurite growth inhibition by antagonistic regulation of RhoA and Rac1. J Neurosci 22:10368–10376.

O'Brien RJ, Kamboj S, Ehlers MD, Rosen KR, Fischbach GD, Huganir RL. 1998. Activity-dependent modulation of synaptic AMPA receptor accumulation. Neuron 21:1067–1078.

Oertle T, van der Haar ME, Bandtlow CE, Robeva A, Burfeind P, Buss A, Huber AB, Simonen M, Schnell L, Brösamle C, Kaupmann K, Vallon R, Schwab ME. 2003. Nogo-A inhibits neurite outgrowth and cell spreading with three discrete regions. J Neurosci 23:5393–5406.

Okamoto K, Bosch M, Hayashi Y. 2009. The roles of CaMKII and F-actin in the structural plasticity of dendritic spines: A potential molecular identity of a synaptic tag? Physiology (Bethesda) 24: 357–366.

Park JI, Frantz MG, Kast RJ, Chapman KS, Dorton HM, Stephany CÉ, Arnett MT, Herman DH, McGee AW. 2014. Nogo receptor 1 limits tactile task performance independent of basal anatomical plasticity. PLoS One 9:e112678. doi: 10.1371/journal.pone.0112678.

Peng X, Kim J, Zhou Z, Fink DJ, Mata M. 2011. Neuronal Nogo-A regulates glutamate receptor subunit expression in hippocampal neurons. J Neurochem 119(6):1183–1193.

Petrinovic MM, Hourez R, Aloy EM, Dewarrat G, Gall D, Weinmann O, Gaudias J, Bachmann LC, Schiffmann SN, Vogt KE, Schwab ME. 2013. Neuronal Nogo-A negatively regulates dendritic morphology and synaptic transmission in the cerebellum. Proc Natl Acad Sci USA 110:1083–1088.

Phair RD, Gorski SA, Misteli T. 2004. Measurement of dynamic protein binding to chromatin in vivo, using photobleaching microscopy. Methods Enzymol 375:393–414.

Pollard TD, Blanchoin L, Mullins RD. 2000. Molecular mechanisms controlling actin filament dynamics in nonmuscle cells. Annu Rev Biophys Biomol Struct 29:545–576.

Raiker SJ, Lee H, Baldwin KT, Duan Y, Shrager P, Giger RJ. 2010. Oligodendrocyte-myelin glycoprotein and Nogo negatively regulate activity-dependent synaptic plasticity. J Neurosci 30:12432–12445.

Ryu J, Liu L, Wong TP, Wu DC, Burette A, Weinberg R, Wang YT, Sheng M. 2006. A critical role for myosin IIb in dendritic spine morphology and synaptic function. Neuron 49:175–182.

Schwab ME. 2010. Functions of Nogo proteins and their receptors in the nervous system. Nat Rev Neurosci 11:799–811.

Star EN, Kwiatkowski DJ, Murthy VN. 2002. Rapid turnover of actin in dendritic spines and its regulation by activity. Nat Neurosci 5: 239–246.

Stoppini L, Buchs PA, Muller D. 1991. A simple method for organotypic cultures of nervous tissue. J Neurosci Methods 37:173–182.

Syken J, Grandpre T, Kanold PO, Shatz CJ. 2006. PirB restricts ocular-dominance plasticity in visual cortex. Science 313:1795–1800.

Tashiro A, Minden A, Yuste R. 2000. Regulation of dendritic spine morphology by the rho family of small GTPases: Antagonistic roles of Rac and Rho. Cereb Cortex 10:927–938.

Tønnesen J, Katona G, Rózsa B, Nägerl UV. 2014. Spine neck plasticity regulates compartmentalization of synapses. Nat Neurosci 17(5):678–85.

Wills ZP, Mandel-Brehm C, Mardinly AR, McCord AE, Giger RJ, Greenberg ME. 2012. The Nogo receptor family restricts synapse number in the developing hippocampus. Neuron 73:466–481.

Yuste R. 2013. Electrical compartmentalization in dendritic spines. Annu Rev Neurosci 36:429–449.

Yuste R, Bonhoeffer T. 2001. Morphological changes in dendritic spines associated with long-term synaptic plasticity. Annu Rev Neurosci 24:1071–1089.

Zagrebelsky M, Schweigreiter R, Bandtlow CE, Schwab ME, Korte M. 2010. Nogo-A stabilizes the architecture of hippocampal neurons. J Neurosci 30:13220–13234.

Zemmar A, Weinmann O, Kellner Y, Yu X, Vicente R, Gullo M, Kasper H, Lussi K, Ristic Z, Luft AR, Rioult-Pedotti M, Zuo Y, Zagrebelsky M, Schwab ME. 2014. Neutralization of Nogo-A enhances synaptic plasticity in the rodent motor cortex and improves motor learning in vivo. J Neurosci 34:8685–8698.

Zito K, Knott G, Shepherd GMG, Shenolikar S, Svoboda K. 2004. Induction of spine growth and synapse formation by regulation of the spine actin cytoskeleton. Neuron 44:321–334.